PCCP

Accepted Manuscript

ROYAL SOCIETY OF CHEMISTRY

www.rsc.org/pccp

Theoretical studies on the absorption spectra of *cis*-[Ru(4,4'-COO-2,2'-bpy)$_2$(X)$_2$]$^{4-}$, (X = NCS, Cl) in water and panchromatic trans-terpyridyl Ru complexes in methanol solution based on time-dependent density functional theory including strong spin-orbit couplings

Kenji Mishima [1)], Takumi Kinoshita [2)], Michitoshi Hayashi [3)], Ryota Jono [1)], Hiroshi Segawa [2)], Koichi Yamashita [1)], and Sheng Hsien Lin [4), 5)]

1) *Department of Chemical System Engineering, Graduate School of Engineering, The University of Tokyo, Tokyo, 113-8656, Japan*

2) *Research Center for Advanced Science and Technology, The University of Tokyo, 4-6-1, Komaba, Meguro-ku, Tokyo, 153-8904, Japan*

3) *Center for Condensed Matter Sciences, National Taiwan University, Taipei 106, Taiwan*

4) *Department of Applied Chemistry, National Chiao Tung University, Hsinchu 30010, Taiwan*

5) *Institute of Atomic and Molecular Sciences, Academia Sinica, P. O. Box 23-166, Taipei 106, Taiwan*

Abstract

In this paper, we theoretically and experimentally investigate the photophysical and chemical characteristics and absorption spectra of various ruthenium complexes in solution used as efficient dye-sensitized solar cells. The target molecules are two

popular complexes, *cis*-[Ru(4,4'-COO-2,2'-bpy)$_2$(X)$_2$]$^{4-}$, (X = NCS, Cl) and trans-terpyridyl Ru. The experimental absorption spectra of these molecules, which show strong spin-orbit (SO) coupling are simulated using first-order perturbation theory based on time-dependent density functional theory and quantum chemistry calculations. It turns out that the theory can simulate the experimental data very well, which indicates that SO coupling is very important and the mixing between singlet and triplet states is strong in these molecules because of the large SO coupling constant of the Ru atom. The exact absorption spectra can only be reproduced by including the perturbation by SO couplings. The physical and chemical differences between *cis*-[Ru(4,4'-COO-2,2'-bpy)$_2$(X)$_2$]$^{4-}$, (X = NCS, Cl) and trans-terpyridyl Ru complexes are elucidated using natural bond orbital and natural transition orbital analyses. From these analyses, we have found that the two kinds of Ru complexes are quite different in terms of photoexitation response and chemical bonding between the central Ru atom and the surrounding ligands.

I. Introduction

Dye-sensitized solar cells (DSSCs) have been extensively investigated experimentally and partially investigated theoretically in recent years in the quest for efficient conversion of solar energy to electricity for the ultimate purpose of achieving a low-carbon society [1 - 3]. Si-based solar cells are widespread nowadays and their photoconversion efficiency is very high, however, the manufacturing cost is high. On the other hand, a fascinating characteristic of DSSCs is the low manufacturing cost; however, their drawback is low photoconversion efficiency. Increased photoconversion efficiency is one of the most important requirements for DSSCs. In fact, the DSSC has been recognized as a versatile and practical solar cell since the first report by Grätzel and coworkers (photoconversion efficiency ≈ 10%) [1]. Since then, various Ru-containing dye molecules, such as *cis*-[Ru(4,4'-COO-2,2'-bpy)$_2$(NCS)$_2$], have been synthesized and the photoconversion efficiencies of the dye-sensitized nanostructured TiO_2 have been measured experimentally. Along with this progress, much attention has been paid to the extension of the absorption threshold of the dye molecules because it is necessary to absorb long-wavelength sunlight (more than near-infrared) that is not efficiently absorbed by conventional organic molecules (usually 200 - 700 nm wavelengths are absorbed by organic molecules), which leads to high photoconversion efficiency. To achieve this aim, modification of the nonanchoring ligands is sometimes used to tailor the absorption spectra of the molecular complexes to maximize the ability to harvest solar radiation [1, 4].

Along with the experimental advancement of syntheses of new high-efficiency dye molecules, theoretical and numerical investigations on such kinds of dye molecules

(e. g., absorption spectra) from the standpoint of electronic structure theory have been making progress in recent years. The current mainstream of the analyses is based on time-dependent density functional theory (TD-DFT) [5]. For example, if we restrict ourselves to N3 dye molecules that are commonly used as sensitizers in the TiO_2-based solar cells [6], pioneering work on the calculation of absorption spectra was performed by Monat *et al*. [7], De Angelis *et al*. [8 - 10], and Adamo *et al*. [11, 12]. To take into account the effect of the solvent around the dye molecules, the polarizable continuum medium (PCM) model [13] with an appropriate dielectric constant of the solvent is usually used. They considered two absorption bands on the lower energy sides from the calculated excitation energies. According to their calculation results, the first absorption band was assigned to a metal-to-ligand charge transfer (MLCT) excitation and the second absorption band was assigned to a ligand-based charge transfer (LBCT) excitation. Their calculations reproduced the experimental absorption spectra fairly well. For Ru complexes containing ligands different from N3 molecules, Aiga *et al*. conducted TD-DFT calculations with the Perdew-Burke-Ernzerhof (PBE) functional for black dye (BD) for the first time [14]. However, their calculations were performed under the assumption of a vacuum environment. Subsequently, for the purpose of a more sophisticated numerical verification of dye molecules attached to the surface of TiO_2, De Angelis *et al*. performed DFT calculations of dye molecule N719 adsorbed on a $(TiO_2)_{38}$ cluster [15].

As for the influence of the different substituent ligands on the absorption spectra, Adamo *et al*. found that the excitation wavelength shifts to longer wavelength when CN ligands are substituted by NCS ligands [11]. Aiga *et al*. found that the first excited state exists at 1101 nm (1.13 eV) in BD, which indicates that the excited state

shifts to a much longer wavelength compared with other Ru complexes [14]. They attributed this tendency to the facts that the highest occupied molecular orbital (HOMO) destabilizes because of the increase in the number of NCS ligands and that the lowest unoccupied molecular orbital (LUMO) of the polypyridyl ligands stabilizes.

Recently, new highly efficient trans-terpyridyl Ru complexes such as shown in Fig. 1 have been synthesized and their absorption spectra and phosphorescence spectra have been measured [16]. The most prominent characteristics of these dye molecules (we call them P1, P2, P3, and P4 dye molecules as shown in Fig. 1) that are different from other dye molecules reported so far are that the former contain a P-substituent as a ligand and that the longest wavelength strong absorption peak (≈1.66 eV - ≈740 nm, one or two orders magnitude more intense than that of the conventional Ru complexes) can seemingly be assigned to the special admittance of a spin-forbidden singlet-to-triplet direct transition of unique panchromatic sensitization. The appearance of such a special peak seems to be qualitatively attributed to the following reason. The conventionally used Ru complexes have a lower spectral response because the main electronic light absorption is from the electronic ground state to a singlet metal-to-ligand charge-transfer (^{1}MLCT) state, which requires a larger energy than that to a triplet metal-to-ligand charge-transfer (^{3}MLCT) state and because the energy loss by relaxation from the ^{1}MLCT state to the ^{3}MLCT state due to the short-lived ^{1}MLCT state through intersystem crossing is estimated to be very large (5000 cm^{-1} - ≈0.6 eV) [17]. The reduction in the spin-exchange energy loss for enhancing the driving force for electron injection to the conduction band (CB) of TiO_2 seems to be achieved from the experimental observations that the Stokes shift considerably is smaller ($\approx 2\times10^3$ cm^{-1}) than those measured for other conventional Ru

complexes such as BD ($\approx 5\times10^3$ cm^{-1}) and that the HOMO-LUMO energy gaps of P1, P2, P3, and P4 molecules are similar to those of BD, which implies the specially admitted singlet-triplet transition allowed by the strong SO coupling. As a consequence, they have achieved a photoconversion efficiency of 11.4 % using the tandem-type DSSC.

Because of these special features of P1, P2, P3, and P4 complexes that can be assumed from the above qualitative reasons by experiments and their promising high photoconversion efficiency as DSSCs, it is necessary to clarify the difference between these dye molecules and conventional dye molecules such as N3 molecules, both theoretically and numerically. First, we have to determine the optimized geometries of these molecules by quantum chemistry calculations. Second, more importantly, because the conventionally used quantum chemistry calculation suites cannot calculate the effect of SO coupling so that the absorption peaks specially arising from SO coupling cannot be simulated, we introduce and utilize first-order perturbation theory based on TD-DFT, where the energy shifts induced by SO couplings are considered as perturbations. By simulating the absorption spectra using the theory, one may be able to verify, for instance, that the absorption spectrum peak at the longest wavelength mentioned above actually corresponds to the specially admitted singlet-triplet transition. Third, we utilize natural bond orbital (NBO) and natural transition orbital (NTO) [18] analyses for the purpose of clarifying the differences and characteristics between P1, P2, P3, and P4 complexes, and the conventional dye molecules such as N3 molecules from the microscopic quantum chemical viewpoint. These analyses are especially useful for investigating molecular characteristics and photophysical response of molecules in more detail than are any other methods.

Recently, Fantacci and coworkers computationally investigated SO coupling-induced spectral broadening of a DX1 dye using the relativistic TD-DFT formalism based on the zero-order regular approximation (ZORA) two-component Hamiltonian [19]. Although our approach, unfortunately, does not describe the exact Hamiltonian, the advantage of our method is that the first-order perturbation theory is much less time-consuming, can be easily extended to larger molecules, and it might be the case that we could include the influence of titanium(IV) oxide in our forthcoming calculations.

The present paper is organized as follows. In Section II, we will show and discuss numerical results, based on the theory developed in the Supporting Information and quantum chemistry calculations. The selected method is one of the currently most utilized DFT functionals (i.e., B3LYP) and basis sets (i.e., LANL2DZ), which have previously proved to agree very well with UV-vis experimental data for various Ru(II) complexes [21 - 25]. In this Section, it will be shown that the theory developed in the Supporting Information dramatically improves the raw absorption spectra calculated by conventional *ab-initio* quantum chemistry suites. In particular, attention will be paid to the longest-wavelength edge of the absorption spectra because of the interest in connection with DSSCs mentioned above. The chemical characteristics of our target dye molecules are analyzed using NBO analysis. In addition, to analyze the excited states contributing to the linear and nonlinear absorptions (in particular, one-photon absorption (OPA) and two-photon absorption (TPA)) and to investigate chemical characteristics of the molecular states involved in these electronic transitions, NTO analysis based on the transition density matrices will be performed [26]. Section III is devoted to concluding remarks. In the Supporting Information, for the present paper to

be self-contained, we introduce and derive the theory for calculation of electronic excitation energies, wave functions, and oscillator strengths (or absorption spectra), taking the SO coupling as a perturbation, for chemical systems having strong SO couplings [20].

II. Numerical Results and Discussion

In this section, we show the numerical results, in particular absorption spectra, obtained using the theory shown in the Supporting Information and quantum chemistry calculation results for our target Ru complexes.

For the nonrelativistic calculations, the quantum chemistry calculations were performed using the GAUSSIAN09 program package [27]. As mentioned in Section I, to take into account the effect of the solvent around the dye molecules, we have used the PCM model [13] with an appropriate dielectric constant for the solvent in all of the following calculations because our experiments were performed in a solvent. The one-electron SO coupling constants used in this work are summarized in Table 1.

On the other hand, in the relativistic quantum chemistry calculations, the geometries optimized nonrelativistically were used as the starting optimized geometries. The relativistic TD-DFT quantum chemistry calculations were carried out based on the ZORA two-component Hamiltonian, as implemented in the ADF package [29 - 31]. The B3LYP exchange-correlation functional and ZORA triple-zeta+polarized (TZP) basis set were used for the calculations. Solvation effects were taken into account using the conductor-like screening model (COSMO) [32].

The optimized geometries of P1, P2, P3, and P4 molecules in methanol solution and *cis*-[Ru(4,4'-COO-2,2'-bpy)$_2$(X)$_2$]$^{4-}$, (X = NCS, Cl) molecules in the gas phase with C1 symmetry (no symmetry constraint) in the singlet ground state (closed-shell singlet S_0) are shown in Fig. 1. The DFT calculations were performed using the B3LYP exchange-correlation functional [33], as implemented in the GAUSSIAN09 program package. In the calculations, a mixed basis set consisting of the LanL2DZ basis set for the Ru atom and the 6-31G** basis set for C, H, N, O, Cl, P, and S atoms was used.

Representative parameters of the optimized geometries of these molecules in the present calculations are given in Table 2. It can be seen that the calculated bond lengths of *cis*-[Ru(4,4'-COO-2,2'-bpy)$_2$(X)$_2$]$^{4-}$, (X = NCS, Cl) molecules reproduce the experimental results fairly well (compare the experimental X-ray data in water solution in [34]). As a general rule, the Ru-Cl bond length is longer than the Ru-N bond length because of the larger atomic radius of Cl than that of N, which leads to the strength of electron donation of the Cl ligands greater than that of the NCS ligands [10]. This tendency is actually reflected in the Ru-Cl bond lengths of the *cis*-[Ru(4,4'-COO-2,2'-bpy)$_2$Cl$_2$]$^{4-}$ molecule being longer than the Ru-N bond lengths of the *cis*-[Ru(4,4'-COO-2,2'-bpy)$_2$(NCS)$_2$]$^{4-}$ molecule. This also leads to the fact that the MLCT excited state energy of the *cis*-[Ru(4,4'-COO-2,2'-bpy)$_2$Cl$_2$]$^{4-}$ molecule (2.02 eV) is lower than that of the *cis*-[Ru(4,4'-COO-2,2'-bpy)$_2$(NCS)$_2$]$^{4-}$ molecule (2.17 eV) because of the increased negative charge on the central Ru atom. The special feature common to P1, P2, P3, and P4 molecules is that the bond lengths of Ru-Cl and Ru-P are a little shorter than those of Ru-Cl in the *cis*-[Ru(4,4'-COO-2,2'-bpy)$_2$Cl$_2$]$^{4-}$ molecule. Furthermore, one can see that the bulkiness of the P-substituent of P1, P2, P3, and P4

molecules significantly affects the Ru-P bond length. If we use the Tolman cone angle listed in Table 3 [35] as a measure of the bulkiness, the bulkiness of the phosphine ligand for P1, P2, P3, and P4 molecules increases in the order P3, P1, P2, and P4 molecules. The Ru-P bond length tends to become longer in the same order, as shown in Table 2. In general, the numerical and experimental structural values agree very well. Therefore, all of the following calculations start from the optimized geometries shown in Fig. 1 and Table 2.

From the NBO analysis for the natural charges on each atom as shown in Table 4, it turns out that the Ru atom is less positively charged than the formal charge of +2, whereas the P atom is strongly positively charged in the cases of P1, P2, P3, and P4 molecules, even though the Ru atom and the surrounding atoms satisfy the 18-electron rule. This is in strong contrast to A1 and A2 molecules where the Ru atom is more positively charged. For example, the natural charges of the Ru atoms of P1, P2, P3, A1, and A2 molecules are -0.412, -0.366, -0.399, 0.129, and 0.089, respectively. On the other hand, the natural charges of P atoms of P1, P2, and P3 molecules are 2.09, 1.84, and 2.04, respectively. What is common to almost all of the molecules is that the N atoms of the ligands are negatively charged and their C atoms are positively charged, which implies the electronegativity of the N atoms larger than the C atoms in the ligands. In addition, from the Wiberg bond indices shown in Table 5, the larger value of the index for the ligand bond, Ru(9)-P(30), amounting to 0.7892, indicates a more pronounced covalent character between the central Ru atom and the phosphine ligand in P2 molecule than between the central Ru atom and the nitrogen atoms of the ligands of A1 and A2 molecules. From these considerations, it can be concluded that the charge

transfer is more efficient or more long-ranged in P1, P2, P3, and P4 molecules than in A1 and A2 molecules.

The absorption spectra obtained by experiment, those estimated by quantum chemistry calculations, and those by quantum chemistry calculations combined with the theory developed in the Supporting Information are shown in Fig. 2. To estimate electronic transition energies ranging from about 1.6 eV to about 2.4 eV, five singlet transitions and five triplet transitions had to be included. This implies that the average energy gap between the neighboring electronic transitions amounts to ≈0.1 eV. The reason for the choice of this number of transitions is that we are mainly concerned with the longest-wavelength edge, as mentioned in the Introduction. Experimentally, from panel (a), it can be seen that the absorption spectra of trans-terpyridyl Ru complexes in methanol solution show two bands in the visible and near-UV regions, and one band in the UV region. The wide band peak between approximately 600 nm and approximately 900 nm is assigned to the MLCT. On the other hand, the narrow band peak around 350 nm is assigned to the $\pi \rightarrow \pi^*$ transition of the terpyridyl ligands. From panel (a), it is observed that there is a small red-shift of the absorption spectrum positions dependent on the different kinds of P-substituents. The amount of the red-shift of the absorption spectra depending on the difference of the P-substituents is affected by the strength of the electron donation by the P-substituents. Most importantly, it should be emphasized that the raw data calculated by quantum chemistry calculation suites such as GAUSSIAN09 can only produce the absorption spectrum peaks for singlet-singlet transitions but cannot produce the oscillator strength and, therefore, the absorption spectrum for singlet-triplet transitions (see panels (b) and (d)) because the conventional quantum chemistry calculation suites do not take into account

the SO couplings of molecules appropriately. Figure 2 actually shows that the raw data calculated by GAUSSIAN09 cannot reproduce the experimental data very well, but the first-order perturbation theory developed in the Supporting Information can reproduce the experimental data very well, for both the spectral intensities and the positions of the spectral peaks (compare panels (a), (b), and (c) for P1 molecule, and panels (a), (d), and (e) for P3 molecule). It should be noted that the tendency of the absorption spectra of these molecules is similar to that of P2 displayed in Fig. 3 in detail below. That is, the gaps between the adjacent peaks are very narrow (≈0.1 eV as estimated above). This may be because the trans-terpyridyl Ru complexes have a strongly electron-donating P-substituent and a smaller number of N-containing ligands than the conventional dye molecules, as clarified below.

Figure 3 compares experimental and numerical absorption spectra at longer wavelength for P2 molecule. If we assume that the molecule is in the gas phase, the quantum chemistry calculations predict that there are several absorption spectrum peaks located at wavelengths slightly longer than those of the experimental data on both the nonrelativistic and relativistic calculation levels (see panels (a) and (f)). On the other hand, if we assume that the molecule is in the methanol solution phase, the raw absorption spectra calculated on both the nonrelativistic and relativistic levels reproduce the experimental data better than in the case of the gas phase, but lead to the misleading result that the oscillator strength for the singlet-triplet transition is zero, as expected (see panels (b) and (g)).

However, absorption spectra including SO couplings calculated by the theory developed in the Supporting Information and obtained from the estimation shown in panel (b) reproduce the experimental data much better (compare the blue solid line in

panel (c) and the black solid line in panel (d)) in terms of spectral intensities. On the other hand, the spectral position was changed insignificantly. In fact, the electronic transition energy at the absorption peak of the lowest transition energy was calculated to be 1.66 eV, which is equal to the experimental value of 1.66 eV [16] as well as close to the raw calculated value of 1.65 eV, even if the transition energy perturbation was included as shown in Eq. (S11). One of the remarkable features is that the shift of the electronic excitation energies is very small for P2 molecule. This is because the interaction between the adjacent electronic excitations that leads to the shift of the electronic excitation energies is small due to the large energy gaps between the adjacent peaks.

The above-mentioned improvement by including SO-coupling originates from the fact that the lowest energy absorption band with a peak around 1.66 eV was assumed to correspond to the specially admitted singlet-triplet transitions allowed by strong SO couplings, as mentioned in Section I, whose intensity is one or two orders of magnitude larger than that of the ordinary Ru dye molecules. In fact, the calculation results presented in panels (b) and (d) show that this is the case. The peak around 1.66 eV in panel (c) arises from the electronically forbidden singlet-triplet transition denoted by the red triangle in panel (b) around 1.66 eV, which has become allowed by the strong SO couplings.

To investigate the effect of the number of transitions involved in the TD-DFT calculation, the absorption spectrum calculated including 15 singlet and 15 triplet transitions is shown in panel (e). Comparing panels (d) and (e), we notice that the relative spectral intensities strongly depend on the number of transitions involved, although the peak positions are almost independent of them.

In panels (h) and (i), we show the absorption spectrum calculated from panel (f) by including SO couplings perturbatively and that calculated by means of the SO coupling-based TD-DFT in methanol solution, respectively. In regard to the excitation energies, all of the cases, panels (d), (e), (h), and (i), are similar and reproduce the experimental result very well. The reason is relatively clear for cases (d), (e), and (h): the calculated absorption peaks without SO couplings for the nonrelativistic (panels (d) and (e)) and relativistic (panel (h)) levels are almost the same (panels (b) and (g), respectively). Therefore, the peak positions perturbed by SO couplings will be almost the same for both of the cases from the argument given above. On the other hand, in regard to the spectral shape or the peak intensities, the nonrelativistic (panel (e)) and relativistic (panel (h) and (i)) calculation results are quite similar.

The absorption spectra for *cis*-$[Ru(4,4'\text{-}COO\text{-}2,2'\text{-}bpy)_2(X)_2]^{4-}$, (X = NCS, Cl) in water are shown in Figs. 4 and 5. To estimate numerically the electronic transition energies ranging from about 2.0 eV up to about 4.4 eV, 50 singlet transitions and 50 triplet transitions had to be included in the TD-DFT calculations. From panel (a) of these figures, it can be seen that the experimentally observed absorption spectra of these molecules in water solution show two bands in the visible and near-UV regions, and one band in the UV region [36, 37], similar to the trans-terpyridyl Ru complexes shown in panel (a) of Fig. 2. The electronic excitations involved in these three absorption bands are identical to those of the trans-terpyridyl Ru complexes shown in panel (a) of Fig. 2. The experimental absorption spectrum indicated by the red line red-shifts compared with calculated absorption spectrum without SO coupling indicated by the blue line in panels (a) of Figs. 4 and 5. But our numerical results including SO coupling shown in panels (c) of Figs. 4 and 5 are more similar to the experimental results compared with

those without SO coupling (in particular, see the absorption peak around 2.4 eV in panel (c) of Fig. 5).

The reason why the observed absorption spectra consist of many electronic excitations and the neighboring peaks are condensed more than those of trans-terpyridyl Ru complexes is that there are two bpy ligands around the central Ru atom and that the energy levels become split by the presence of carboxyl groups for N3 dye molecule. This in turn implies that there are a smaller number of electronic excitations and that the neighboring peaks are sparse in P1, P2, P3, and P4 molecules because of the smaller number of bpy ligands and carboxyl-groups around the central Ru atom in these molecules.

To analyze the excited states contributing to the linear and nonlinear absorptions (in particular, OPA and TPA) and to investigate the chemical characteristics of the molecular states involved in these electronic transitions, NTO analyses were performed. The numerical results of NTO analyses are shown in Figs. 6 and 7. Figure 6 is for P2 molecule in methanol solution and Fig. 7 is for *cis*-$[Ru(4,4'\text{-}COO\text{-}2,2'\text{-}bpy)_2Cl_2]^{4-}$ molecule in water solution. In the figures, we only concentrate on the two lowest transitions involved in all of the electronic transitions because of the greater interest in the long-wavelength electronic transitions. From Fig. 6, one can see that OPA is dominant in the lowest singlet-triplet transition whereas TPA dominates in the second lowest singlet-nearly singlet transition (the excited singlet state contributes 98.25 % in the transition). In addition, we can see that the initial state is mainly localized on a Ru d(π) orbital and its slight contribution comes from the terpyridyl ligands. The final state is mainly localized on the terpyridyl ligands. On the other hand, from Fig. 7, it is seen that OPA is dominant in the lowest singlet-triplet

transition whereas TPA is almost negligible in the second lowest singlet-triplet transition. This is because the two excited states have almost the same energy in such a way that the excited state molecular orbitals are very similar to each other. In addition, we can see that the initial state is mainly localized on a Ru d(π) orbital and its slight contribution comes from the ligands. As mentioned above, both in Fig. 6 and in Fig. 7, the electrons are concentrated near the Ru atom and are slightly delocalized by the nitrogen and carbon 2p character originating from the antibonding ligand orbitals in the initial higher occupied states, and they are spread out and are near the carboxyl groups in the final state, which indicates that in fact MLCT takes place efficiently at the longer wavelength and that the electrons are injected into the CB of TiO_2 efficiently because the molecules are anchored to the surface of TiO_2 by the carboxyl groups. Furthermore, the fact that the electronic density is concentrated on the ligands and that it is not found on the P-substituent in the final state in Fig. 6 for P2 molecule confirms the assumption that the atomic group consisting of Ru atom, Cl atoms, and the P-substituent of P2 molecule can be considered as a chemical "*entity.*" It was verified that this also applies to other trans-terpyridyl Ru complexes such as P1, P3, and P4 molecules in contrast to other typical Ru complexes. Nevertheless, it can be seen that wave functions of the electron and the hole have an approximately odd symmetry in Fig. 6 and Fig. 7. In this regard, the P-substituted molecules and the ordinary dye molecules are similar to each other.

From the NTO analysis, it also turns out that a considerable enhancement of the transition dipole moment (thus, the oscillator strength) of the first excited state of P2 compared with that of *cis*-$[Ru(4,4'\text{-}COO\text{-}2,2'\text{-}bpy)_2Cl_2]^{4-}$ molecules from the experimental data [16] provides effective charge transfer over longer distances in the

former molecule. This enhancement was also predicted from NBO analysis that the P-substituent in P2 molecule is strongly electron-donating, which is absent in *cis*-$[Ru(4,4'\text{-}COO\text{-}2,2'\text{-}bpy)_2(X)_2]^{4-}$, (X = NCS, Cl) molecules. This effect provides the sparse absorption spectra, leading to the long-wavelength absorption edge in the panchromatic trans-terpyridyl Ru complexes such as P2 molecule investigated in detail in the present paper.

III. Conclusion

In conclusion, we have successfully reproduced the absorption spectra of the popularly used *cis*-$[Ru(4,4'\text{-}COO\text{-}2,2'\text{-}bpy)_2(X)_2]^{4-}$, (X = NCS, Cl) in water solution and trans-terpyridyl Ru complexes in methanol solution. The calculation method for such kinds of molecules that have strong SO couplings was the first-order perturbation theory based on TD-DFT and DFT quantum chemistry method. From the Wiberg bond indices, the larger value of the index for the ligand bond between the Ru and the P atoms indicates a more pronounced covalent character between the central Ru atom and the phosphine ligand in P2 molecule than between the central Ru atom and the nitrogen atoms of the ligands of A1 and A2 molecules. From these considerations, it can be concluded that the charge transfer is more efficient or more long-ranged in P1, P2, P3, and P4 molecules than in A1 and A2 molecules. Furthermore, from NTO analysis, we have found that the former have small TPA because of similar hole states and small energy gaps (i. e., the peaks of the absorption spectra are condensed) whereas the latter have an almost equal contribution of OPA and TPA because of very different hole states and large energy gaps (i. e., the peaks of the absorption spectra are sparse).

This implies that the nonlinear absorption may be contaminated in the absorption spectra of trans-terpyridyl Ru complexes.

To achieve the efficient conversion of solar energy to electricity, the extension of the absorption threshold to the longer wavelength of the dye molecules is the most important issue. The successful threshold extension of trans-terpyridyl Ru complexes was originated from the fact that the introduction of a strongly electron-donating P-substituent enhances the transition dipole moment of the first excited state, thus the oscillator strength, and long-range charge transfer stabilizes the transition and provides the sparse absorption spectra, leading to the long-wavelength absorption edge.

Recently, time-resolved emission decays from N719/TiO_2 films in various electrolytes were investigated experimentally [38]. The issue is whether the electron injection is effectively taking place from the singlet or triplet states of the dye molecule to the CB of TiO_2. In addition, the electronically excited states have to be long-lived [38]. In a similar context, to scrutinize the photophysical dynamics occurring in the Ru complexes investigated in the present work, detailed calculations of internal conversion rates, intersystem crossing rate between singlet and triplet states, electron injection rates from the singlet and triplet states, and the simulation of the time-resolved absorption or emission decay are now underway.

Acknowledgements

This work was supported by Funding Program for World-Leading Innovative R&D on Science and Technology (FIRST) "Development of Organic Photovoltaics toward a Low-Carbon Society," Cabinet Office, Japan.

References

[1] B. O' Regan and M. Grätzel, Nature, **353** (1991) 737.

[2] M. Grätzel, Nature, **414** (2001) 338.

[3] J. M. Kroon, N. J. Bakker, H. J. P. Smit, P. Liska, K. R. Thampi, P. Wang, S. M. Zakeeruddin, M. Grätzel, A. Hinsch, S. Hore, U. Würfel, R. Sastrawan, J. R. Durrant, E. Palomares, H. Pettersson, T. Gruszecki, J. Walter, K. Skupien, G. E. Tulloch, Prog. Photovolt. Res. Appl., **15** (2007) 1.

[4] S. M. Zakeeruddin, M. K. Nazeeruddin, P. Pechy, F. P. Rotzinger, R. HumpuryBaker, K. Kalyanasundaram, M. Grätzel, V. Shklover, and T. Haibach, Inorg. Chem., **36** (1997) 5937.

[5] A. Dreuw and M. Head-Gordon, Chem. Rev., **105** (2005) 4009.

[6] X. Yang, and M. H. Baik, J. Am. Chem. Soc., **128** (2006) 7476.

[7] J. E. Monat, J. H. Rodriguez, J. K. McCusker, J. Phys. Chem. A, **106** (2002) 7399.

[8] S. Fantacci, F. De Angelis, A. Selloni, J. Am. Chem. Soc., **125** (2003) 4381.

[9] F. De Angelis, S. Fantacci, and A. Selloni, Chem. Phys. Lett., **389** (2004) 204.

[10] F. De Angelis, S. Fantacci, A. Selloni, and M. K. Nazeeruddin, Chem. Phys. Lett., **415** (2005) 115.

[11] J. –F. Guillemoles, V. Barone, L. Joubert, and C. Adamo, J. Phys. Chem. A, **106** (2002) 11354.

[12] M. Rekhis, F. Labat, O. Ouamerali, I. Cofini, and C. Adamo, J. Phys. Chem. A, **111** (2007) 13106.

[13] J. Tomasi, B. Mennucci, and R. Cammi, Chem. Rev., **105** (2005) 2999.

[14] F. Aiga and T. Toda, J. Mol. Struc., **658** (2003) 24.

[15] F. De Angelis, S. Fantacci, A. Selloni, M. Grätzel, and M. K. Nazeeruddin, Nano Lett., **7** (2007) 3189.

[16] T. Kinoshita, J. T. Dy, S. Uchida, T. Kubo, and H. Segawa, Nat. Photonics, **7** (2013) 535.

[17] K. Kalyanasundaram, *Photochemistry of polypyridine and porphyrin complex.* (Academic press, London, 1992).

[18] R. L. Martin, J. Chem. Phys., **118** (2003) 4775.

[19] S. Fantacci, E. Ronca, and F. D. Angelis, J. Phys. Chem. Lett., **5** (2014) 375.

[20] K. Nozaki, J. Chin. Chem. Soc., **53** (2006) 101.

[21] H. Wolpher, S. Sinha, J. X. Pan, A. Johansson, M. J, Lundqvist, P. Persson, R. Lomoth, J. Bergquist, L. C. Sun, V. Sundstrom, B. Akermark, and T. Polivka, Inorg. Chem., **46** (2007) 638.

[22] F. S. Han, M. Higuchi, and D. G. Kurth, J. Am. Chem. Soc., **130** (2008) 2073.

[23] C. Nouarner-Rassin, F. Chaignon, C. She, D. Stockwell, E. Blart, P. Buvat, T. Lian, and F. Odobel, J. Photochem. Photobiol., A **192** (2007) 56.

[24] I. Gillaizeau-Gauthier, F. Odobel, M. Alebbi, R. Argazzi, E. Costa, C. A. Bignozzi, P. Qu, and G. J. Meyer, Inorg. Chem., **40** (2001) 6073.

[25] M. Nilsing, S. Lunell, P. Persson, and L. Ojamae, Surf. Sci., **582** (2005) 49.

[26] J. B. Asbery, Y.-Q. Wang, E. Hao, H. N. Ghosh, and T. Lian, Res. Chem. Intermed., **27** (2001) 393.

[27] M. J. Frisch, *et al*., *GAUSSIAN 09*, Gaussian, Inc., Wallingford, CT, 2009.

[28] S. Fraga, K. M. S. Saxena, and J. Karowowski, *Handbook of Atomic Data. Physical Sciences Data* Vol. 5. Elsevier, Amsterdam, The Netherlands, 1976.

[29] G. te Velde, F. M. Bickelhaupt, E. J. Baerends, C. Fonseca Guerra, S. J. A. van Gisbergen, J. G. Snijder, T. Ziegler, Chemistry with ADF, J. Comp. Chem., **22** (2001) 931.

[30] ADF 2012, *SCM, Theoretical Chemistry*, Vreije Universiteit: Amsterdam, The Netherlands, http://www.scm.com (2013).

[31] C. Fonseca Guerra, J. G. Snijder, G. te Velde, E. J. Baerends, Theor. Chem. Acc., **99** (1998) 391.

[32] C. C. Pye and T. Ziegler, Theor. Chem. Acc., **101** (1999) 396.

[33] A. D. Becke, J. Chem. Phys., **98** (1993) 5648.

[34] V. Shklover, Yu. E. Ovchinnikov, L. S. Graginsky, S. M. Zakeeruddin, and M. Grätzel, Chem. Mater., **10** (1998) 2533.

[35] C. A. Tolman, Chem. Rev., **77** (1977) 313.

[36] V. Shklover, Md. K. Nazeeruddin, S. M. Zakeeruddin,, C. Barbe, A. Kay, T. Haibach, W. Steurer, R. Hermann, H.-U. Nissen, and M. Grätzel, Chem. Mater., **9** (1997) 430.

[37] Md. K. Nazeeeruddin, S. M. Zakeeruddin, R. Humpry-Baker, M. Jirousek, P. Liska, N. Vlachopoulos, V. Shklover, C.-H. Fisher, and M. Grätzel, Inorg. Chem., **38** (1999) 6298.

[38] S. E. Koops, B. C. O'Regan, P. R. F. Barnes, and J. R. Durrant, J. Am. Chem. Soc., **131** (2009) 4808

Figure captions

Fig. 1 Molecular structures in the singlet ground state of P1, P2, P3, and P4 molecules, and *cis*-[Ru(4,4'-COO-2,2'-bpy)$_2$(X)$_2$]$^{4-}$, (X = NCS, Cl) molecules. In the figure, *cis*-[Ru(4,4'-COO-2,2'-bpy)$_2$(NCS)$_2$]$^{4-}$ and *cis*-[Ru(4,4'-COO-2,2'-bpy)$_2$Cl$_2$]$^{4-}$ molecules are abbreviated as A1 and A2, respectively.

Fig. 2 (a) Experimental absorption spectra of P1, P2, P3, and P4 molecules in methanol solvent. (b) Raw absorption spectra calculated using the quantum chemistry calculation package for P1 molecule. The black solid bar is for the singlet-singlet transition and the red solid bar is for the singlet-triplet transition. (c) Absorption spectra including SO couplings calculated by the theory developed in the Supporting Information and obtained from panel (b). Note the good agreement with experiment. (d) Raw absorption spectra calculated using the quantum chemistry calculation package for P3 molecule. The black solid bar is for the singlet-singlet transition and the red solid bar is for the singlet-triplet transition. (e) Absorption spectra including SO couplings calculated by the theory developed in the Supporting Information and obtained from panel (d). Note the good agreement with experiment.

Fig. 3 Absorption spectra of P2 molecule calculated using GAUSSIAN09 in the gas phase (panel (a)) and in methanol solution (panel (b)). Panel (c) shows the experimental absorption and emission spectra of P2 molecule in methanol solution, with being the red line being the emission spectrum (phosphorescence spectrum), with blue line being the absorption spectrum measured at 77 K, and the dashed line being the

absorption spectrum measured at RT. Panel (d) shows the absorption spectrum calculated using the theory developed in the Supporting Information, including five singlet and five triplet transitions. Panel (e) corresponds to that calculated including 15 singlet and 15 triplet transitions. Panels (f) and (g) show the absorption spectra calculated by means of the scalar relativistic (SR) TD-DFT in the gas phase (panel (f)) and in methanol solution (panel (g)). Panel (h) shows the absorption spectrum calculated from panel (g) by including SO couplings perturbatively. Panel (i) shows the absorption spectrum calculated by means of the SO coupling-based TD-DFT (SOC-TDDFT) in methanol solution. All of the spectra are interpolated using Gaussian functions with σ =0.06 eV.

Fig. 4 Absorption spectra of *cis*-[Ru(4,4'-COO-2,2'-bpy)$_2$Cl$_2$] molecule in water solution. (a) Experimental (red line) and numerical (blue line) absorption spectra [10]. (b) Numerical raw absorption spectra. (c) Numerical absorption spectrum including SO couplings calculated by the theory developed in Sec. II and obtained from quantum chemistry calculations of panel (b).

Fig. 5 Absorption spectra of *cis*-[Ru(4,4'-COO-2,2'-bpy)$_2$(NCS)$_2$] molecule in water solution. (a) Experimental (red line) and numerical (blue line) absorption spectra [10]. (b) Numerical raw absorption spectra. (c) Numerical absorption spectrum including SO couplings calculated using the theory developed in Supporting Information and obtained from the quantum chemistry calculations of panel (b). The peak around 2.4 eV is interpolated by Gaussian functions with σ =0.06 eV.

Fig. 6 NTOs of P2 molecule in methanol solution for the two lowest electronic transition energies. The shown energies are the electronic transition energies and the numbers of OPA and TPA indicate the fraction of OPA and TPA transitions in the corresponding transitions, respectively. White, gray, red, orange, blue, and green spheres represent H, C, O, P, N, and Ru atoms, respectively.

Fig. 7 NTOs of *cis*-$[Ru(4,4'\text{-}COO\text{-}2,2'\text{-}bpy)_2Cl_2]^{4-}$ molecule in water solution for the two lowest electronic transition energies. The shown energies are the electronic transition energies and the numbers of OPA and TPA indicate the fraction of OPA and TPA transitions in the corresponding transitions, respectively. White, gray, red, yellowish green, blue, and green spheres represent H, C, O, Cl, N, and Ru atoms, respectively.

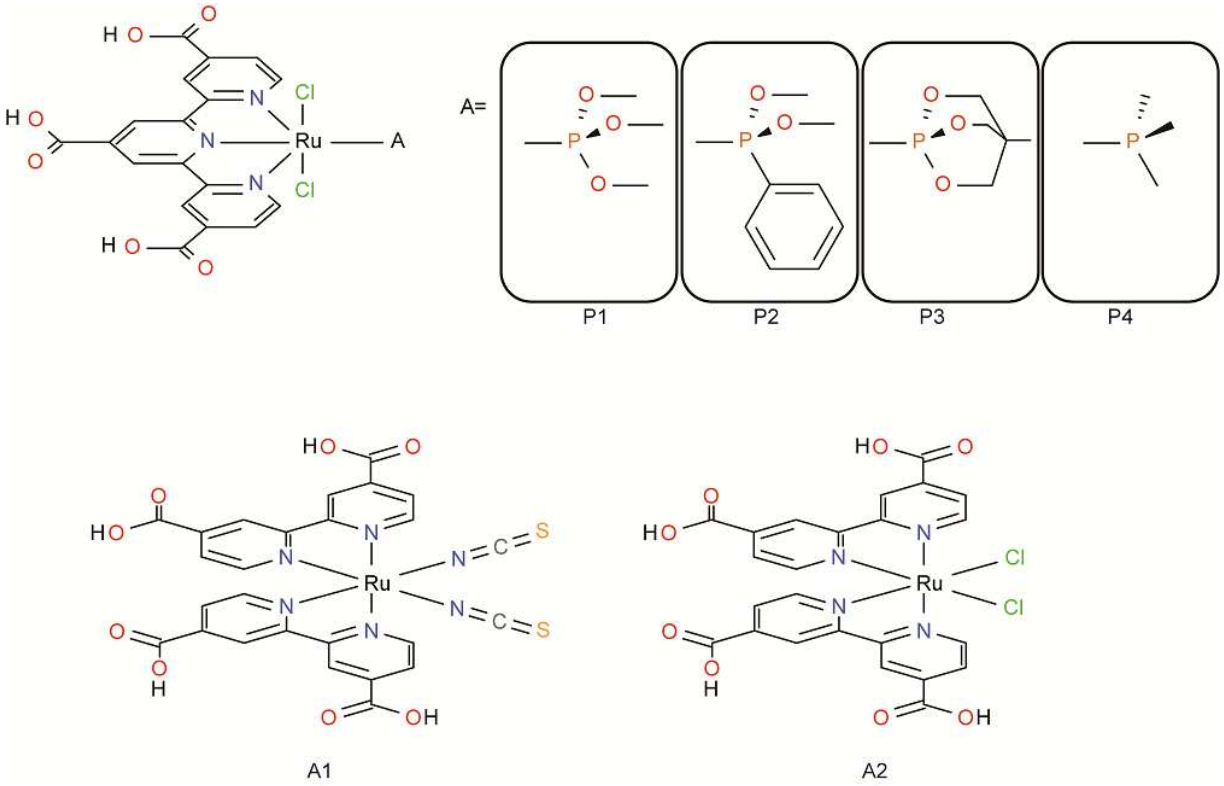

Fig. 1 K. Mishima *et al*.

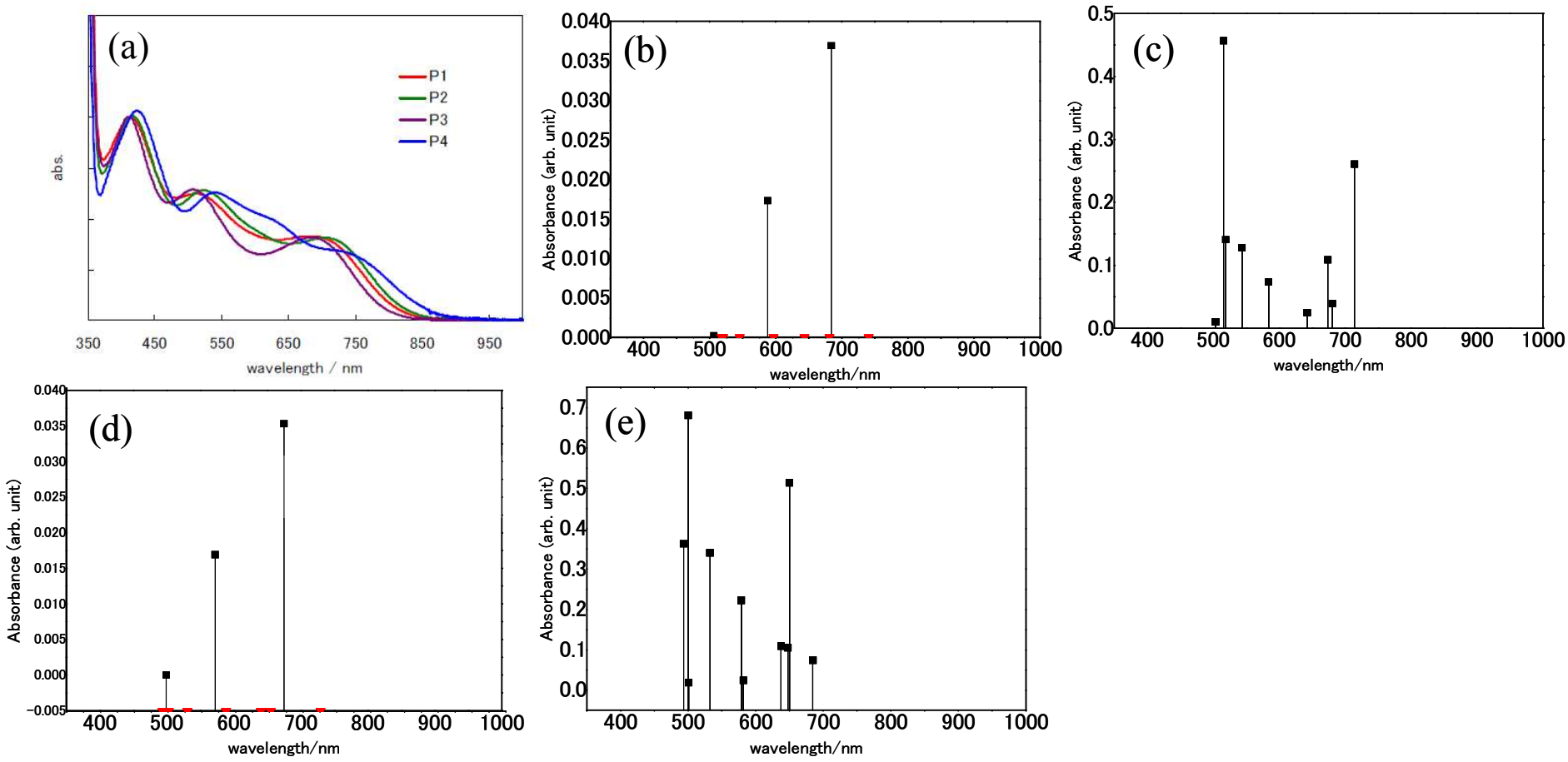

Fig. 2 K. Mishima *et al*.

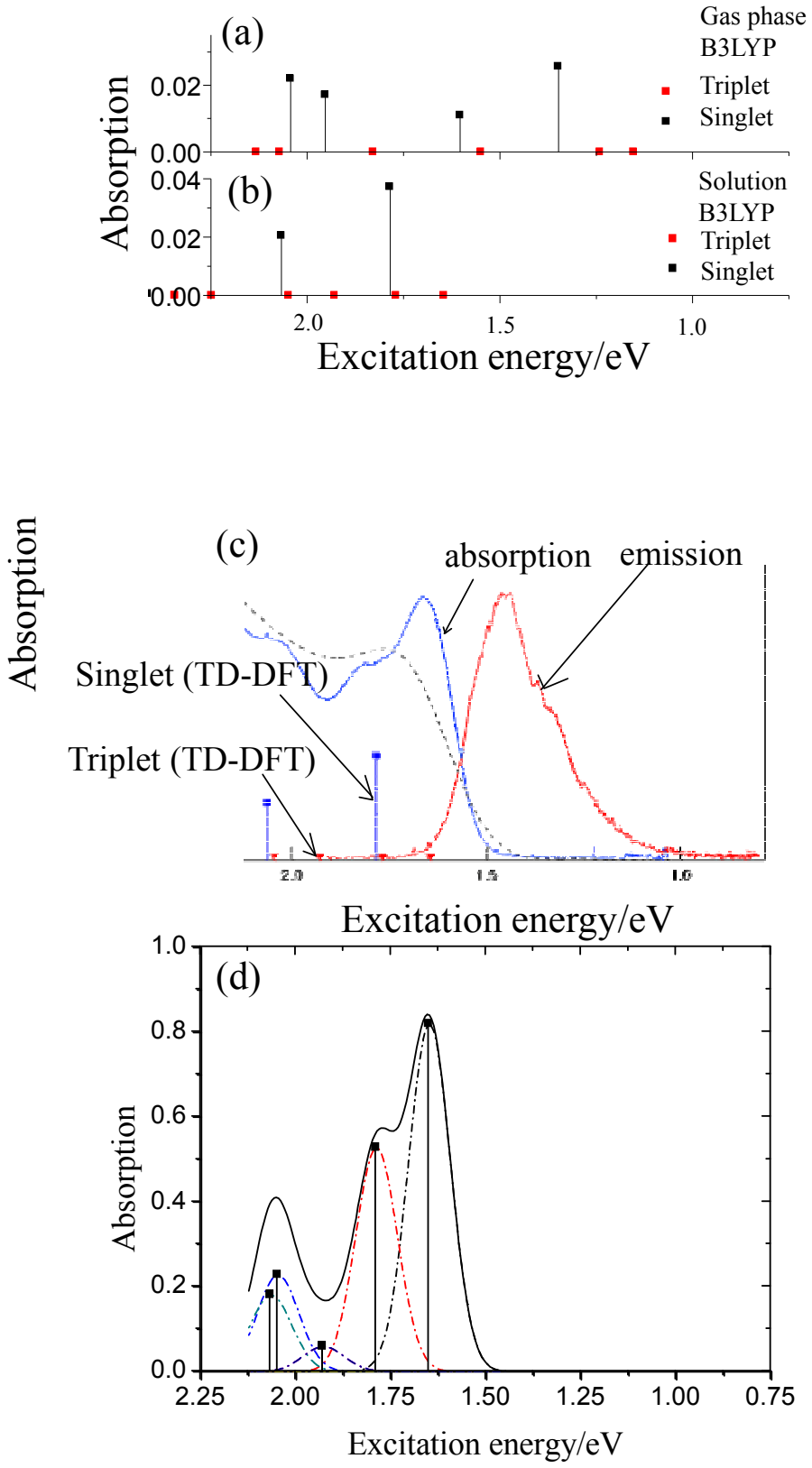

Fig. 3 K. Mishima *et al.*

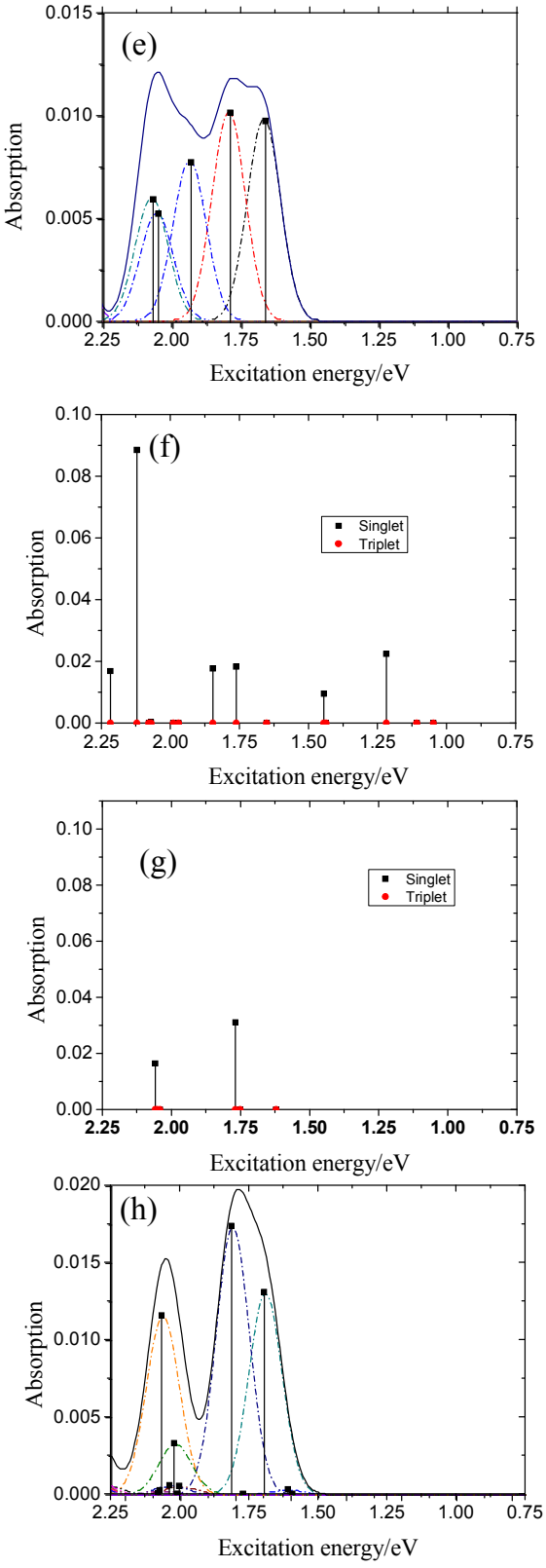

Fig.3 (continued) K. Mishima *et al.*

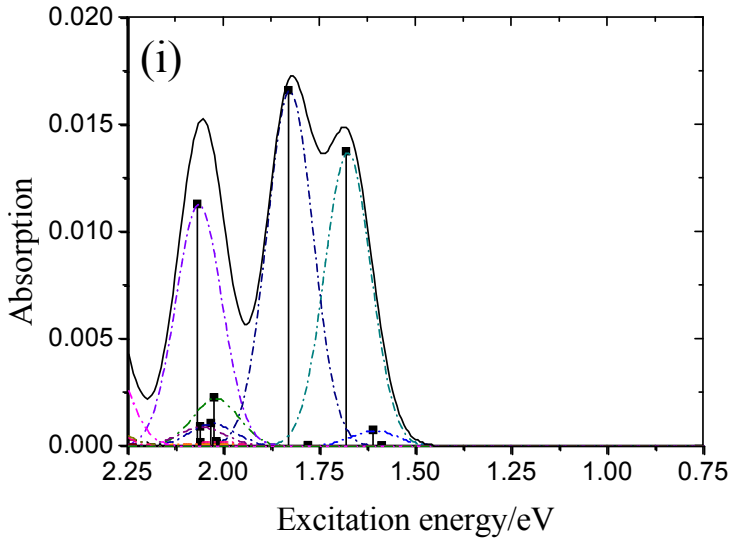

Fig. 3 (continued) K. Mishima *et al*.

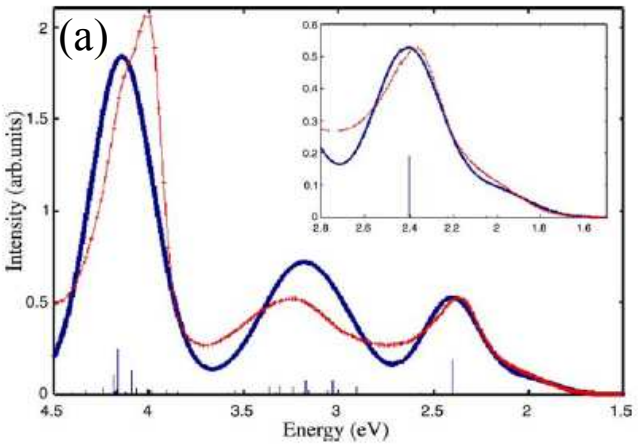

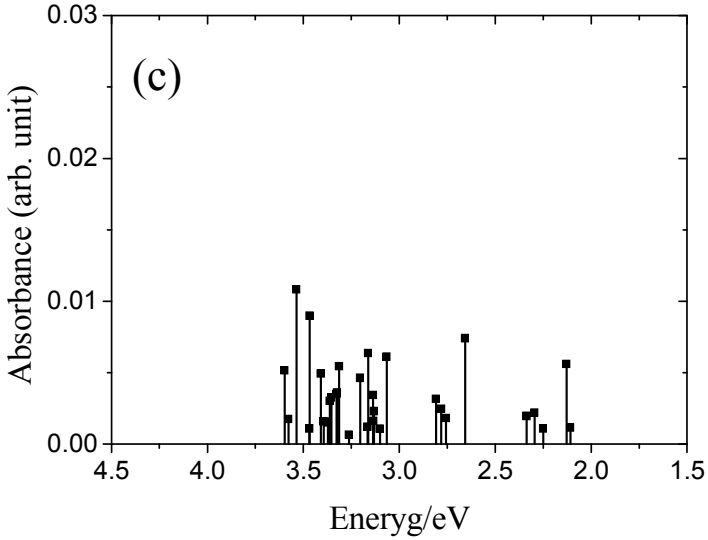

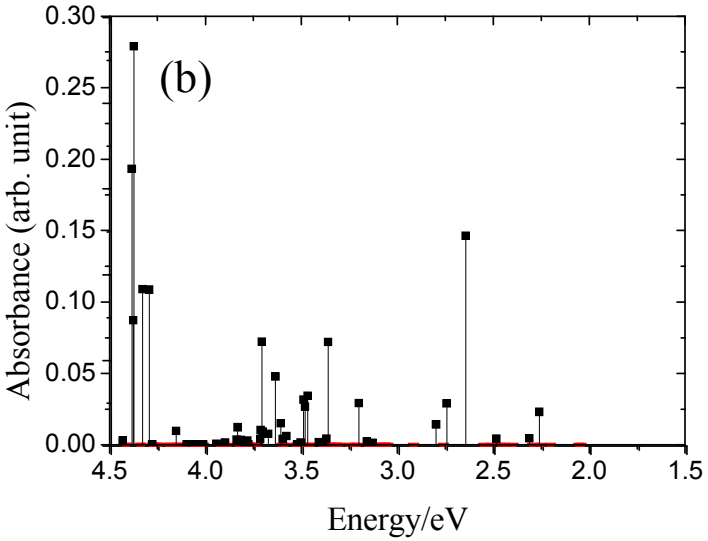

Fig4. K. Mishima *et al.*

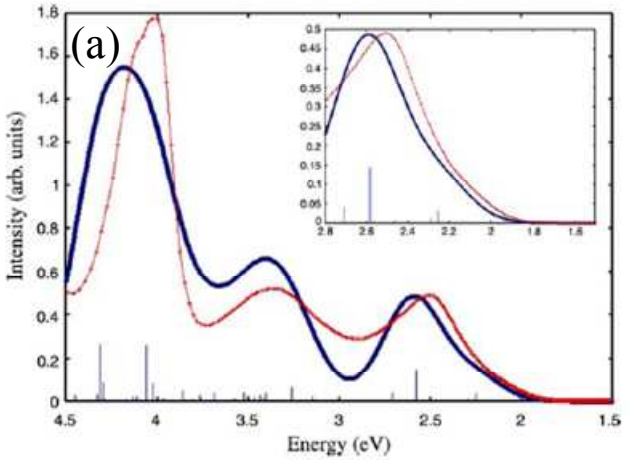

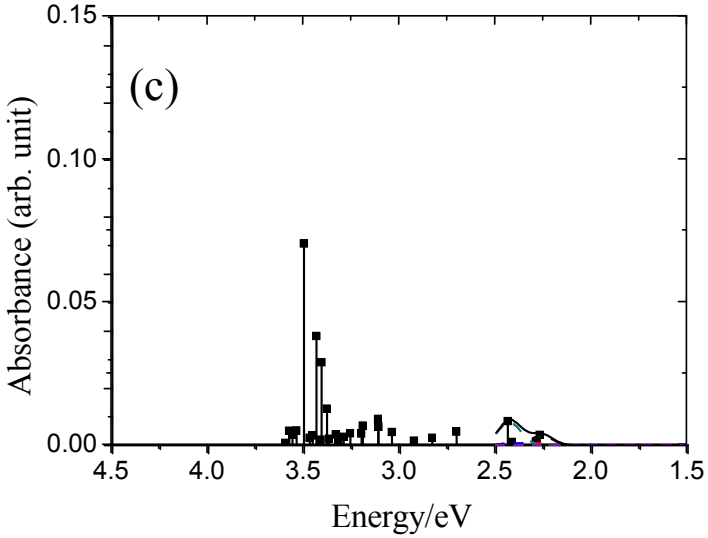

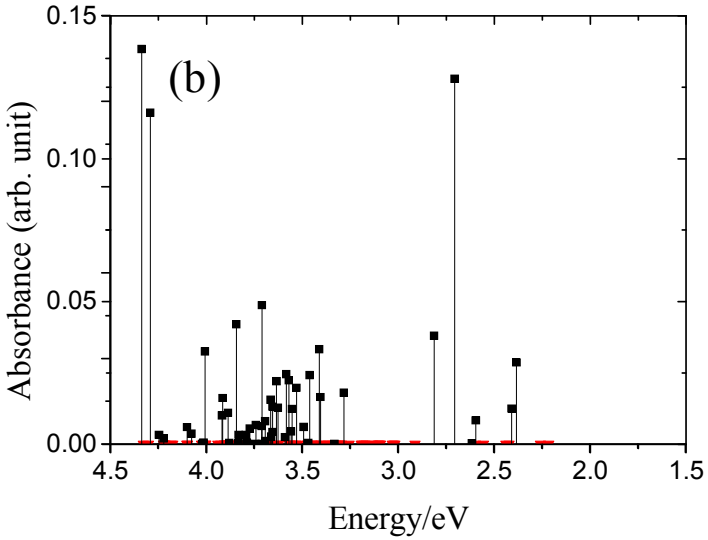

Fig5. K. Mishima *et al.*

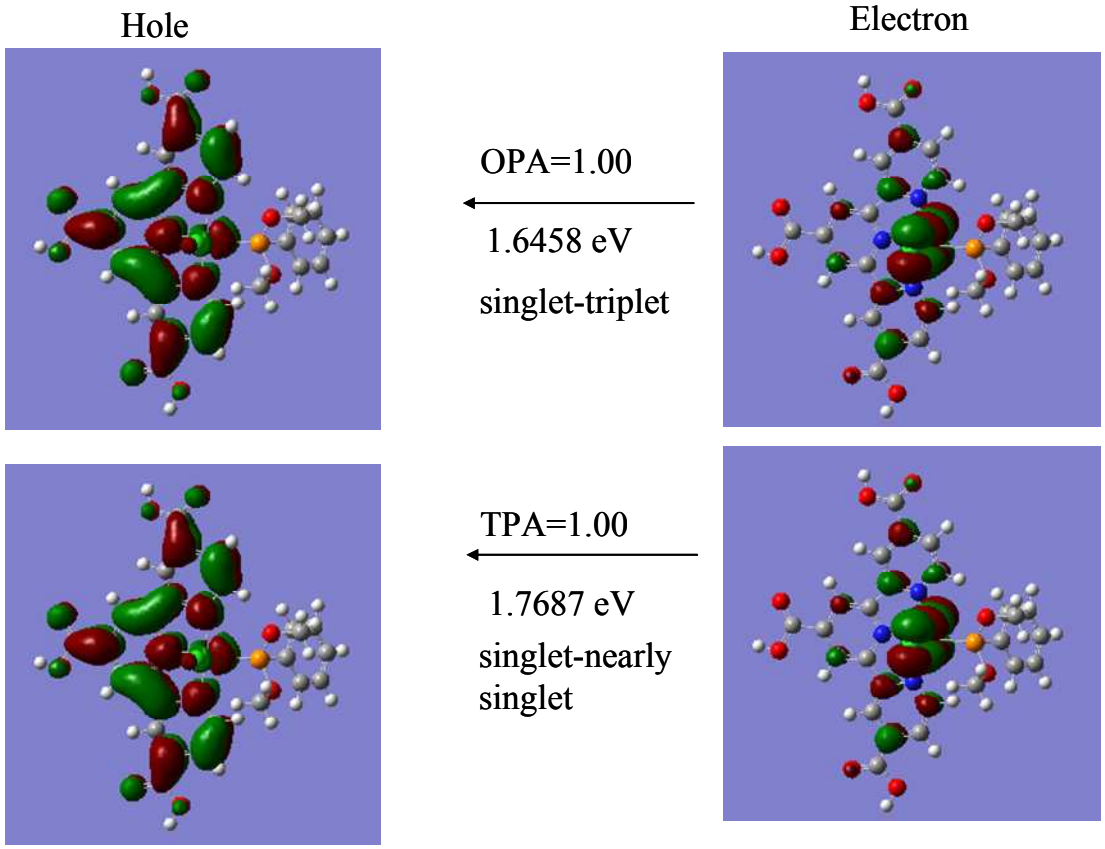

Fig6. K. Mishima *et al*.

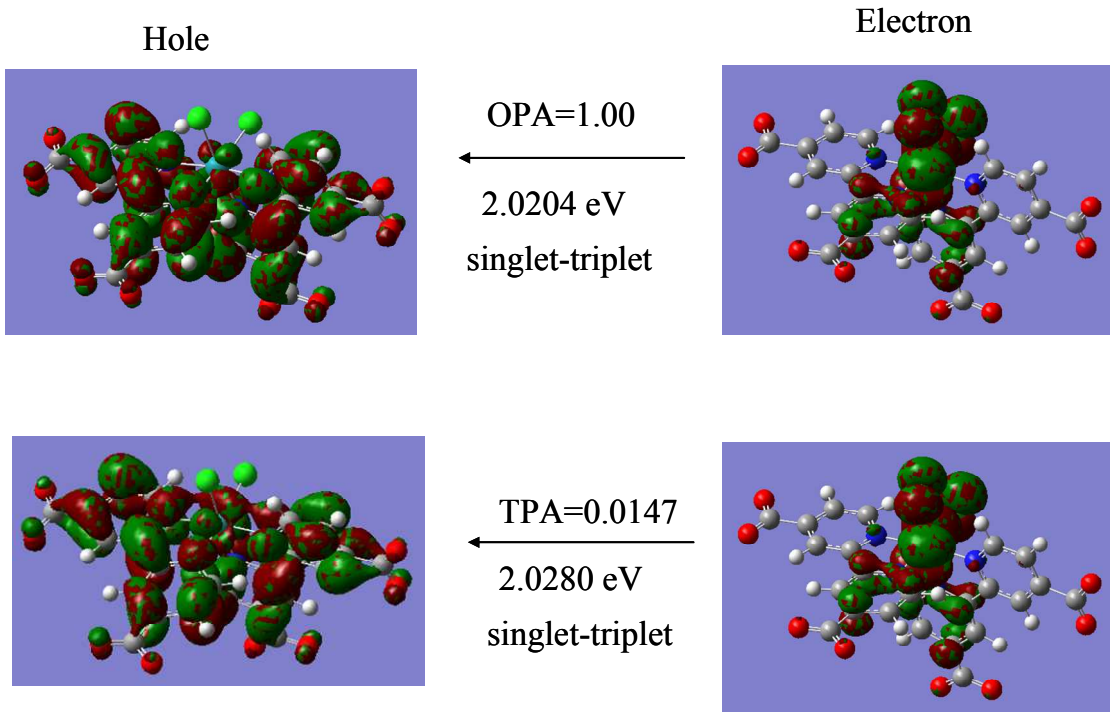

Fig7. K. Mishima *et al*.

Table 1. One-electron SO coupling constants used in this work [28].

Atom	configuration	ζ_c/cm^{-1}
C	$(2p)^2$	32.4
N	$(2p)^3$	77.8
Ru	$(4d)^6$	1081
S	$(3p)^4$	365.08
O	$(2p)^4$	154.29
Cl	$(3p)^5$	550.81
P	$(3p)^3$	229.45

Table 2. Bond distances in the unit of Å around Ru atom for P1, P2, P3, P4, A1, and A2 molecules. In this Table, *cis*-[Ru(4,4'-COO-2,2'-bpy)$_2$(NCS)$_2$]$^{4-}$ and *cis*-[Ru(4,4'-COO-2,2'-bpy)$_2$Cl$_2$]$^{4-}$ molecules are abbreviated as A1 and A2, respectively. The atoms are those numbered in Fig. 1.

Molecule	Ru(12)-N(4)	Ru(12)-N(13)	Ru(12)-N(29)	Ru(12)-Cl(40)	Ru(12)-Cl(41)	Ru(12)-P(42)
P1	2.125	2.1189	2.0189	2.4964	2.4944	2.3444

Molecule	Ru(9)-N(4)	Ru(9)-N(10)	Ru(9)-N(26)	Ru(9)-Cl(28)	Ru(9)-Cl(29)	Ru(9)-P(30)
P2	2.1208	2.1259	2.0191	2.4917	2.4989	2.3607

Molecule	Ru(12)-N(4)	Ru(12)-N(13)	Ru(12)-N(29)	Ru(12)-Cl(40)	Ru(12)-Cl(41)	Ru(12)-P(42)
P3	2.1213	2.1218	2.0172	2.4935	2.4912	2.3076

Molecule	Ru(1)-N(8)	Ru(1)-N(21)	Ru(1)-N(46)	Ru(1)-Cl(54)	Ru(1)-Cl(3)	Ru(1)-P(2)
P4	2.0855	2.0787	1.9645	2.4738	2.4943	2.52

Molecule	Ru(1)-N(6)	Ru(1)-N(38)	Ru(1)-N(17)	Ru(1)-N(41)	Ru(1)-N(37)	Ru(1)-N(24)
A1	2.0899	2.0994	2.1043	2.0994	2.0899	2.1043

Molecule	Ru(1)-N(6)	Ru(1)-Cl(50)	Ru(1)-N(17)	Ru(1)-Cl(51)	Ru(1)-N(37)	Ru(1)-N(24)
A2	2.0683	2.5624	2.1032	2.5624	2.0683	2.1032

Table 3. Tolman cone angles of phosphine ligands of P1, P2, P3, and P4 molecules [35].

Molecule	Ligand	Tolman cone angle (degree)
P1	$P(OMe)_3$	107
P2	P(OMe)2Ph	115
P3	$P(OCH_2)_3CMe$	101
P4	PMe_3	118

Table 4. Natural charges of atoms contained in P2, A1, and A2 molecules.

Molecule	Ru(9)	N(4)	N(10)	N(26)	Cl(28)	Cl(29)	P(30)
P2	-0.3665	-0.3353	-0.3360	-0.3157	-0.4756	-0.4775	1.8425

Molecule	Ru(1)	N(6)	N(38)	N(17)	N(41)	N(37)	N(24)
A1	0.1285	-0.3543	-0.4318	-0.3667	-0.4318	-0.3542	-0.3667

Molecule	Ru(1)	N(6)	Cl(50)	N(17)	Cl(51)	N(37)	N(24)
A2	0.0889	-0.3490	-0.5918	-0.3774	-0.5918	-0.3490	-0.3774

Table 5. Wiberg bond indices of ligand bonds of P2, A1, and A2 molecules.

Molecule	Ru(9)-N(4)	Ru(9)-N(10)	Ru(9)-N(26)	Ru(9)-Cl(28)	Ru(9)-Cl(29)	Ru(9)-P(30)
P2	0.5244	0.5184	0.5344	0.6952	0.6853	0.7892

Molecule	Ru(1)-N(6)	Ru(1)-N(38)	Ru(1)-N(17)	Ru(1)-N(41)	Ru(1)-N(37)	Ru(1)-N(24)
A1	0.5515	0.5672	0.5223	0.5672	0.5515	0.5223

Molecule	Ru(1)-N(6)	Ru(1)-Cl(50)	Ru(1)-N(17)	Ru(1)-Cl(51)	Ru(1)-N(37)	Ru(1)-N(24)
A2	0.5754	0.5832	0.5135	0.5832	0.5754	0.5135

Supporting Information

for

Theoretical studies on the absorption spectra of *cis*-$[Ru(4,4'\text{-}COO\text{-}2,2'\text{-}bpy)_2(X)_2]^{4-}$, (X = NCS, Cl) in water and panchromatic trans-terpyridyl Ru complexes in methanol solution based on time-dependent density functional theory including strong spin-orbit couplings

Kenji Mishima [1)], Takumi Kinoshita [2)], Michitoshi Hayashi [3)], Ryota Jono [1)], Hiroshi Segawa [2)], Koichi Yamashita [1)], and Sheng Hsien Lin [4), 5)]

1) *Department of Chemical System Engineering, Graduate School of Engineering, The University of Tokyo, Tokyo, 113-8656, Japan*

2) *Research Center for Advanced Science and Technology, The University of Tokyo, 4-6-1, Komaba, Meguro-ku, Tokyo, 153-8904, Japan*

3) *Center for Condensed Matter Sciences, National Taiwan University, Taipei 106, Taiwan*

4) *Department of Applied Chemistry, National Chiao Tung University, Hsinchu 30010, Taiwan*

5) *Institute of Atomic and Molecular Sciences, Academia Sinica, P. O. Box 23-166, Taipei 106, Taiwan*

Theory: First-order perturbation theory for molecules having strong SO couplings

The theory of absorption spectra for molecules having strong SO coupling has been developed by Nozaki [S1]. It is based on the first-order perturbation theory of SO coupling matrix elements. For the Ru complexes in mind, the first-order perturbation theory is accurate enough, because the largest one electron spin-orbit coupling constant for Ru atom in the $(4d)^6$ configuration (1081 cm^{-1} ~ 0.13 eV) is only about 10 % of the first electronic excitation energy. In order for the present paper to be self-contained, we will briefly introduce the theory and point out some missing formulas in the original theory [S1].

From the degenerate perturbation theory, the *k*-th molecular wavefunction perturbed by SO coupling, $\left|\Psi_k^{SO}\right\rangle$, is given by

$$\left|\Psi_k^{SO}\right\rangle = \sum_{\substack{\sigma=S,T \\ i}} c_{k,i}^{\sigma} \left|\Psi_i'^{\sigma}\right\rangle \qquad \text{(S1)}$$

where σ is the spin index, *S* and *T* stand for singlet and triplet states, respectively, $\left|\Psi_i'^{\sigma}\right\rangle$ is the *i*-th unperturbed wavefunction of the molecule, and $c_{k,i}^{\sigma}$ is the coefficient of the linear combination of the perturbed molecular wavefunction. From the general perturbation theory for degenerate quantum states, the perturbation energy due to SO coupling, E_{SO}, is expressed as

$$\left(\left\langle\Psi'\right|\hat{H}_{SO}\left|\Psi'\right\rangle - E_{SO}I\right)C = 0, \qquad \text{(S2)}$$

where $\hat{H}_{SO}$ is the SO coupling Hamiltonian, $\boldsymbol{I}$ is the unit matrix, and $\boldsymbol{C}$ is the coefficient column vector for $c_{k,i}^{\sigma}$. As shown in FigS1., under the assumption of the ground-state electronic wavefunction, $\left|\Phi_g^{\sigma}\right\rangle$, consisting of a single determinant of Kohn-Sham orbitals with spin index σ, we can approximate the *k*-th unperturbed

molecular excited-state electronic wavefunction, $\left|\Psi_k'^{\sigma}\right\rangle$, as a linear combination of one-electron excitation configurations from the *p*-th molecular orbital (MO) with spin σ (ϕ_p^{σ}) to the *q*-th MO with spin σ (ϕ_q^{σ}), $\left|\Phi_k^{\sigma}(p\to q)\right\rangle$:

$$\left|\Psi_k'^{\sigma}\right\rangle=\sum_{p=1}^{occ}\sum_{q=occ+1}a_{pqk}^{\sigma}\left|\Phi_k^{\sigma}(p\to q)\right\rangle, \tag{S3}$$

where a_{pqk}^{σ} is the coefficient of the linear combination of the unperturbed molecular excited-state electronic wavefunction in terms of $\left|\Phi_k^{\sigma}(p\to q)\right\rangle$.

The SO coupling matrix elements between the *k*-th and the *l*-th unperturbed wavefunctions, $\left\langle\Psi_k'^{\sigma}\left|\hat{H}_{SO}\right|\Psi_l'^{\sigma'}\right\rangle$, can be approximately represented by the sum of one-electron one-center SO integrals between these electronic configurations, as shown in FigS2. [S2, S3]:

$$\left\langle\Psi_k'^{\sigma}\left|\hat{H}_{SO}\right|\Psi_l'^{\sigma'}\right\rangle=\sum_{p=1}^{occ}\sum_{q=occ+1}\sum_{r=occ+1}a_{pqk}^{\sigma}a_{prl}^{\sigma'}\left\langle\Phi_k^{\sigma}(p\to q)\left|\hat{H}_{SO}\right|\Phi_l^{\sigma'}(p\to r)\right\rangle$$

$$+\sum_{q=occ+1}\sum_{p=1}^{occ}\sum_{r=1}^{occ}a_{pqk}^{\sigma}a_{rql}^{\sigma'}\left\langle\Phi_k^{\sigma}(p\to q)\left|\hat{H}_{SO}\right|\Phi_l^{\sigma'}(r\to q)\right\rangle. \tag{S4}$$

To evaluate one-electron one-center SO integrals presented in FigS2. ((a) is for singlet transition and (b) is for triplet transition), we will use natural atomic orbitals ($\left|\chi_j\right\rangle$, NAO) to expand molecular orbitals:

$$\left|\phi\right\rangle=\sum_j b_j\left|\chi_j\right\rangle, \tag{S5}$$

where $|\phi\rangle$ is the atomic orbital (AO) and b_j is the coefficient of the representation of the linear combination of AO, $|\phi\rangle$, in terms of NAO's, $|\chi_j\rangle$. Here, Kohn-Sham ground state, $|\Phi_g^\sigma\rangle$, can be expressed as

$$|\Phi_g^\sigma\rangle = \frac{1}{\sqrt{N!}}|\phi_1 \cdots \phi_N|, \tag{S6}$$

where $|\cdots|$ denotes the Slater determinant. NAO's are optimal (maximum occupancy) effective AO's in the molecular environment. The use of NAO's is very advantageous compared with that of other types of AO's. For example, NAO's allow us to avoid the basis set dependence of calculation results because one specific NAO is localized one-center orbital that maintains intra- and inter-atomic orthogonality to the remaining NAO's. Using NAO's, the SO integral, $\langle \Psi_k'^\sigma | \hat{H}_{SO} | \Psi_l'^{\sigma'} \rangle$, can be evaluated as

$$\langle \Psi_k'^\sigma | \hat{H}_{SO} | \Psi_l'^{\sigma'} \rangle = \sum_{p=1}^{occ} \sum_{q=occ+1} \sum_{r=occ+1} a_{pqk}^\sigma a_{prl}^{\sigma'} \sum_m \sum_n b_{qm} b_{rn} \Xi_{mn}^{\sigma\sigma'}(v)$$

$$+ \sum_{q=occ+1} \sum_{p=1}^{occ} \sum_{r=1}^{occ} a_{pqk}^\sigma a_{rql}^{\sigma'} \sum_m \sum_n b_{pm} b_{rn} \Xi_{mn}^{\sigma\sigma'}(o). \tag{S7}$$

Here, for example,

$$\Xi_{mn}^{\sigma\sigma'}(v) = \frac{1}{2}\left(\langle \chi_{d_{xy}}^\alpha | \hat{H}_{SO} | \chi_{d_{xz}}^\beta \rangle + \langle \chi_{d_{xy}}^\beta | \hat{H}_{SO} | \chi_{d_{xz}}^\alpha \rangle \right), \tag{S8}$$

if the valence orbital contributing to the SO integrals is *d*-orbital. Owing to the fact that NAO's with the intra-atomic orthogonality are similar to the Slater orbitals in shape, for example, the SO integral in terms of NAO's given in Eq. (S8),

$\left\langle \chi_{d_{xy}}^{\alpha} \middle| \hat{H}_{SO} \middle| \chi_{d_{xz}}^{\beta} \right\rangle$, can be approximated by the SO integral between the corresponding Slator orbitals,

$$\left\langle \chi_{d_{xy}}^{\alpha} \middle| \hat{H}_{SO} \middle| \chi_{d_{xz}}^{\beta} \right\rangle \sim \zeta_c \left\langle \chi_{d_{xy}}^{\alpha} \middle| \hat{H}_{SO} \middle| \chi_{d_{xz}}^{\beta} \right\rangle = \frac{1}{2}\zeta_c , \tag{S9}$$

where ζ_c is the on-electron SO coupling constant for an effective SO potential resulting from the screening effect of the nuclear charge by the closed shell electrons [S4 – S8]. The values of ζ_c are given in [S4].

By solving the eigenvalue problem of Eq. (S2), one obtains the *k*-th molecular wavefunction perturbed by SO coupling, $\left|\Psi_k^{SO}\right\rangle$, given by Eq. (S1). Using the perturbed wavefunctions, the oscillator strength proportional to the strength of the absorption spectra, *f*, is given by

$$f = \frac{8\pi^2 m_e}{3he^2}\tilde{\nu}_{em}\left|\left\langle \Psi_g \middle| \hat{\vec{\mu}} \middle| \Psi_k^{SO} \right\rangle\right|^2 = \frac{8\pi^2 m_e}{3he^2}\tilde{\nu}_{em}\left|\sum_{\substack{\sigma=S,T \\ i}} c_{k,i}^{\sigma}\left\langle \Psi_g \middle| \hat{\vec{\mu}} \middle| \Psi_i'^{\sigma} \right\rangle\right|^2 , \tag{S10}$$

where m_e is the mass of the electron, *h* is the Planck's constant, *e* is the unit charge, $\hat{\vec{\mu}}$ is the transition dipole moment operator, $\tilde{\nu}_{em}$ is the wavenumber of the incident electromagnetic wave, and $\left|\Psi_g\right\rangle$ is the ground-state electronic molecular wavefunction. The transition energy perturbed by the SO coupling, E_k^{new}, is given by the ordinary first-order perturbation theory:

$$E_k^{new} = E_k^{(0)} + E_{k,SO}^{(1)} , \tag{S11}$$

where $E_k^{(0)}$ is the zero-th order energy and $E_{k,SO}^{(1)}$ is the first-order perturbation energy calculated by Eq. (S2).

References for Supporting Information

[S1] K. Nozaki, J. Chin. Chem. Soc., **53** (2006) 101.

[S2] Z. A. Siddique, Y. Yamamoto, T. Ohno, and K. Nozaki, Inorg. Chem., **42** (2003) 6366.

[S3] Z. A. Siddique, T. Ohno, K. Nozaki, and T. Tsubomuira, Inorg. Chem., **43** (2004) 663.

[S4] S. Fraga, K. M. S. Saxena, and J. Karowowski, *Handbook of Atomic Data. Physical Sciences Data* Vol. 5. Elsevier, Amsterdam, The Netherlands, 1976.

[S5] M. Blume and R. E. Watson, Proc. Roy. Soc. (London) **A270** (1963) 127.

[S6] M. Blume and R. E. Watson, Proc. Roy. Soc. (London) **A271** (1964) 565.

[S7] A. Misetich and T. Buch, J. Chem. Phys., **41** (1964) 2524.

[S8] D. S. McClure, J. Chem. Phys., **20** (1952) 682.

Figure Captions for Supporting Information

FigS1. Pictorial representations of Kohn-Sham molecular ground state with spin index σ $\left|\Phi_g^\sigma\right\rangle$ (usually, because the ground state is the singlet state, $\sigma = S$), and singly excited configurations to singlet ($\left|\Phi_k^\sigma(p \to q)\right\rangle$) and triplet states ($\left|\Phi_k^{\sigma'}(p \to q)\right\rangle$).

FigS2. Pictorial representation of the one-electron one-center SO integral, $\left\langle \Phi_k^\sigma(p \to q)\right|\hat{H}_{SO}\left|\Phi_l^{\sigma'}(p \to r)\right\rangle$, between the electronic configurations, $\Phi_k^\sigma(p \to q)$ and $\Phi_k^{\sigma'}(p \to r)$.

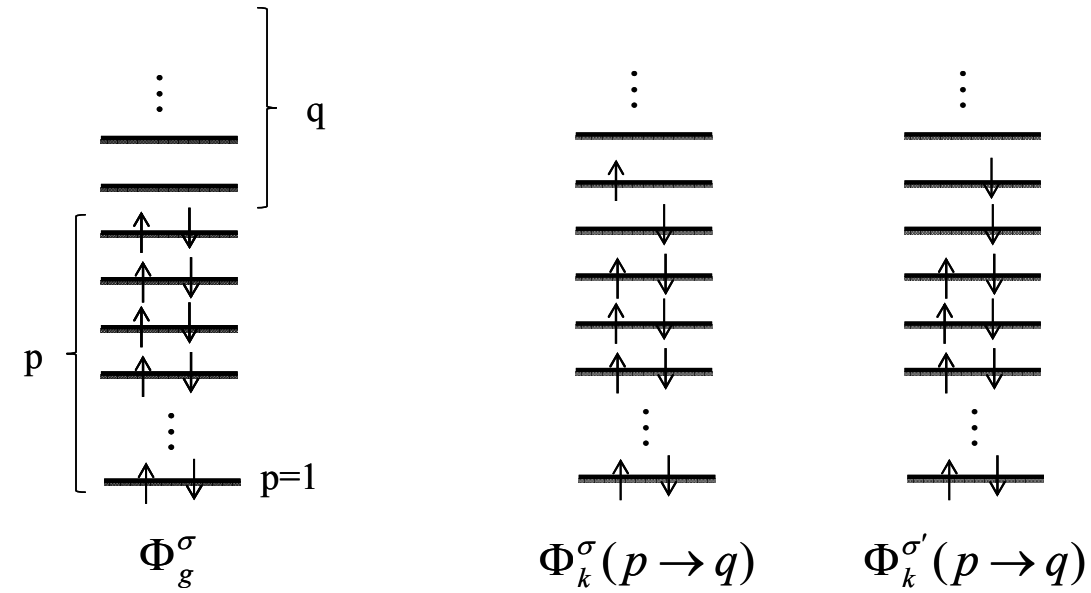

FigS1. K. Mishima *et al.*

$$\left\langle \Phi_k^{\sigma}(p \to q) \middle| \hat{H}_{SO} \middle| \Phi_l^{\sigma'}(p \to r) \right\rangle$$

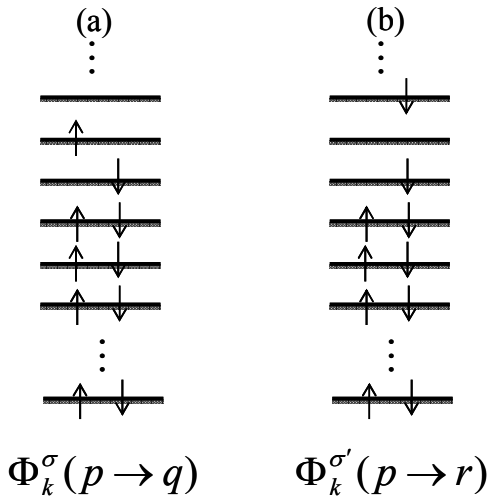

FigS2. K. Mishima *et al*.